Jpn. J. Appl. Phys. Vol. 40 (2001) pp. 49–53
Part 1, No. 1, January 2001

Device Simulation of Grain Boundaries in Lightly Doped Polysilicon Films and Analysis of Dependence on Defect Density

Mutsumi KIMURA*, Satoshi INOUE, Tatsuya SHIMODA and Toshiyuki SAMESHIMA[1]

Base Technology Research Center, Seiko Epson Corporation, 281 Fujimi, Nagano 399-0293, Japan
[1]*Division of Electric and Information Engineering, Tokyo University of Agriculture and Technology, 2-24-16 Nakamachi, Koganei 184-8588, Japan*

(Received August 8, 2000; accepted for publication October 19, 2000)

Device simulations of grain boundaries in lightly doped polysilicon films have been performed. Dependence of the energy band, carrier density, potential barrier and electric conductivity on the defect density and grain size was carefully investigated. As a result, the mechanism of the carrier transportation has been clarified. The boundary defects not only trap and reduce free carriers, but also form the potential barrier and interfere with the carrier movement. As the defect density increases, in the case of the small grain size, first, the space-charge regions spread over the entire grain. Next, while the potential barrier remains the same, the lowest energy of the conduction band from the Fermi level (E_c-E_f) increases, and the carrier density decreases. Finally, E_c-E_f becomes the highest and remains the same. On the other hand, in the case of the large grain size, before the space-charge regions spread over the entire grain, E_c-E_f at the grain boundary reaches its maximum. Therefore, even if the defect density increases further, the potential barrier remains the same, and the carrier density remains high. By comparing the experimental and simulated electric conductivity, the defect density can be extracted.

KEYWORDS: device simulation, grain boundary, lightly dope, polysilicon, defect, potential barrier, electric conductivity

1. Introduction

In laser-crystallized polysilicon (poly-Si) thin-film transistors (TFTs), the channels are formed in the laser-crystallized poly-Si films, which have few defects in the grains and many defects at the grain boundaries. In order to understand how these TFTs work, it is necessary to clarify the mechanism of the carrier transportation in these poly-Si films. One of the most effective methods for clarifying this mechanism is the evaluation of lightly doped poly-Si films.[1–5] In the evaluation of lightly doped poly-Si films, no voltage is applied along the poly-Si film depth, and no carriers concentrate at the oxide-silicon interface. Therefore, the effect of the oxide-silicon interface on the carrier transportation is negligible, and the effect of the grain boundaries on the carrier transportation is dominant. Moreover, since the change of the potential and carrier density along the poly-Si film depth is negligible, a two dimensional subject can be reduced to a one dimensional subject. Furthermore, with respect to the experiment, since only poly-Si films with some contact pads are required, it is easy to fabricate them.

To date, research has been conducted to analyze the lightly doped poly-Si films.[6–9] However, since this research was based on analytical methods, there were some assumptions and approximations that caused errors. Therefore, the objective of this paper is to perform device simulation in order to analyze the lightly doped poly-Si films precisely and determine the mechanism of the carrier transportation in the poly-Si films precisely. The method to extract the defect density will also be shown.

2. Device Simulation of Grain Boundaries

Figure 1 shows the carrier transportation in the lightly doped poly-Si film with boundary defects. Grain size is defined by d, and there are four grains and five grain boundaries. This structure can be assumed to be a part of the longer poly-Si film. Donor-type dopants are implanted. Dopant density is $1 \times 10^{19}\,\mathrm{cm}^{-3}$, and dopant energy, E_d, is 0.04 eV below the lowest energy of the conduction band, E_c. The generation of the carriers by dopants in this poly-Si film corresponds to that by application of gate voltage in the poly-Si TFT. Defect states are caused by dangling bonds and located at grain boundaries. The boundary defects are assumed to be distributed in the plane. If the boundary defects are point defects such as atomic holes, line defects such as dislocations or plane defects such as stacking faults, the following discussions are applicable. The energy distribution of the boundary defects is Gaussian, as follows:

$$N_t(E) = N_l \exp\{-[(E - E_1)/E_2]^2\}. \quad (1)$$

Here, N_t and E are the density of defect states and the energy in the energy gap, respectively. The total defect density is determined by integrating eq. (1) along the energy. The defect density varies in the plane density of the order of 10^{11}–$10^{14}\,\mathrm{cm}^{-2}$, which corresponds to the volume density of the order of 10^{17}–$10^{20}\,\mathrm{cm}^{-3}$ if the boundary defects are assumed to be distributed uniformly throughout the en-

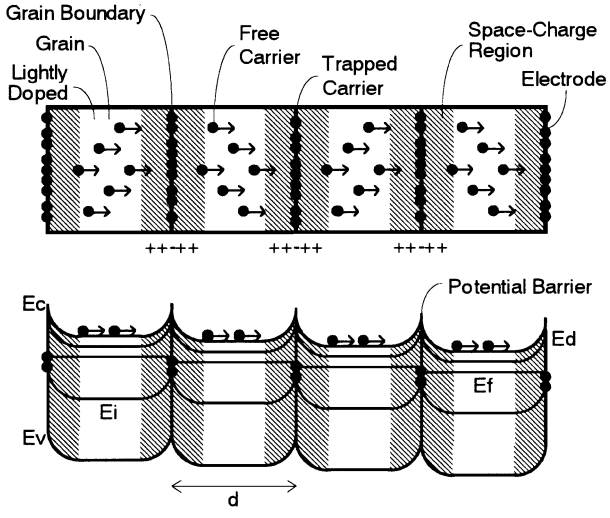

Fig. 1. Carrier transportation in the lightly doped poly-Si film with boundary defects.

*E-mail address: kimura.mutsumi@exc.epson.co.jp

tire poly-Si film. For the as-crystallized poly-Si film, the defect density is very high. $E_1 = 0\,\mathrm{eV}$, which means that the boundary defects are distributed around the midgap in the energy band, and $E_2 = 0.15\,\mathrm{eV}$, which means that the Gaussian width is 0.3 eV. The boundary defects distributed around the midgap can be confirmed by the high potential barrier measured in an experiment.[5] The acceptor-like state is defined as a trap state that is neutral or negatively charged according to the Fermi level. The donor-like state is defined as a trap state that is neutral or positively charged according to the Fermi level. It is assumed that the defect density of the acceptor-like states and donor-like states are the same. This leads to a flat-band condition without the application of voltage. The voltage applied to both sides of the poly-Si film is 0.1 V.

The donor-type dopants are ionized and generate free electron carriers in the conduction band. The free carriers are trapped at the boundary defects and decrease. On the other hand, the boundary defects are charged negatively. In order to preserve charge neutrality, positive charges equal to negative charges at the boundary defects are induced on both sides of the grain boundary. That is, the free carriers decreases on both sides of the boundary, and space-charge regions are created by the positive charges of the dopant ions. These space-charge regions form a potential barrier at the boundary. The potential barrier influences the occupation probability of the boundary defects, and the potential barrier and occupation probability are decided self-consistently. As a result, the boundary defects influence the carrier transportation using two mechanisms. First, the boundary defects trap the free carriers and reduce them. Second, the boundary defects form the potential barrier and interfere with the movement of the free carriers. Only the thermally activated free carriers can travel through the potential barrier.

The device simulation can handle all the above-mentioned phenomena without any approximations.[10–12] In the device simulation, generally, the following equations are utilized:

$$\Delta\psi = -\rho/\varepsilon \tag{2}$$

$$\nabla\cdot(-n_\mathrm{n}\mu_\mathrm{n}\boldsymbol{E} - D_\mathrm{n}\nabla n_\mathrm{n}) - G = 0 \tag{3}$$

$$\nabla\cdot(n_\mathrm{p}\mu_\mathrm{p}\boldsymbol{E} - D_\mathrm{p}\nabla n_\mathrm{p}) - G = 0. \tag{4}$$

Equation (2) is the Poisson equation to calculate the potential. Equations (3) and (4) are the continuous equations for electrons and holes, respectively. These equations are based on the drift-diffusion model and utilized to calculate the carrier transportation. The following equations are also utilized:

$$n_\mathrm{n} = N_\mathrm{c}\exp[-(E_\mathrm{c} - E_\mathrm{f})/(kT)] \tag{5}$$

$$n_\mathrm{p} = N_\mathrm{v}\exp[-(E_\mathrm{f} - E_\mathrm{v})/(kT)]. \tag{6}$$

Equations (5) and (6) are the carrier density equations for electrons and holes, respectively. These equations are utilized to relate the carrier density with the quasi Fermi level. In these equations, instead of the Fermi-Dirac distribution, the Maxwell-Boltzmann distribution is utilized. Therefore, in the case that the lowest energy of the conduction band or the highest energy of the valence band is similar to the Fermi level, these equations are not valid. This occurs in the middle of the grain for large grain size and low defect density. However, since the electric conductivity is high in this region, the effect on the total electric conductivity is not significant. Therefore, these equations can be utilized. In this paper, the following equations are utilized:

$$n_\mathrm{d} = N_\mathrm{d}(1/\{1 + \exp[(E_\mathrm{f} - E_\mathrm{d})/(kT)]\}) \tag{7}$$

$$n_\mathrm{ta} = \int N_\mathrm{ta}(E)(1/\{1 + \exp[(E - E_\mathrm{f})/(kT)]\})\mathrm{d}E \tag{8}$$

$$n_\mathrm{td} = \int N_\mathrm{td}(E)(1/\{1 + \exp[(E_\mathrm{f} - E)/(kT)]\})\mathrm{d}E. \tag{9}$$

Equations (7), (8) and (9) are the occupation probability equations for donors, acceptor-like states and donor-like states, respectively. The following equation is also utilized and substituted into eq. (2):

$$\rho = q(-n_\mathrm{n} + n_\mathrm{p} + n_\mathrm{d} - n_\mathrm{ta} + n_\mathrm{td}). \tag{10}$$

In the device simulation, the structure is divided into many meshes, and eqs. (2)–(10) are formulated at each mesh. By iterating to solve these equations and achieving convergence, the carrier density and potential can be calculated. Finally, the energy band, carrier density, potential barrier, electric conductivity, etc. can be calculated.

3. Dependence on the Defect Density

Dependence of the energy band, carrier density, potential barrier and electric conductivity on the defect density and

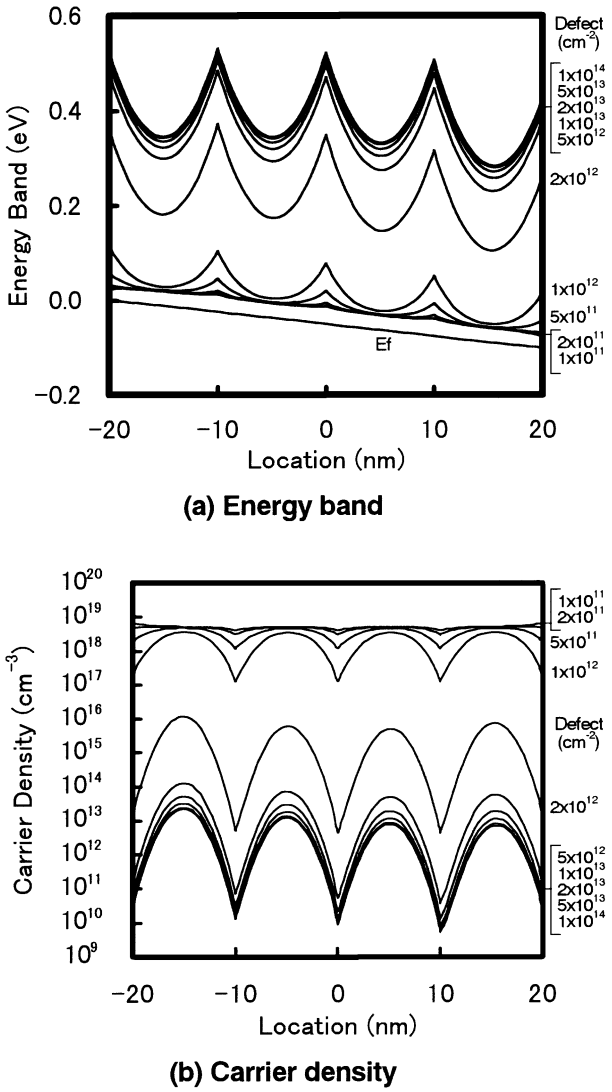

Fig. 2. Dependence of the (a) energy band and (b) carrier density with variations in the defect density for a grain size of 10 nm.

grain size was carefully investigated.

Figure 2 shows the dependence of the (a) energy band and (b) carrier density with variations in the defect density for a grain size of 10 nm. Figures 3 and 4 show those for grain sizes of 20 nm and 50 nm, respectively. In Figs. 2(a), 3(a) and 4(a), the lowest energy of the conduction band, E_c, for each defect density is shown by overlapping the Fermi level, E_f. It is found that the potential barrier is formed at the grain boundary. In Figs. 2(b), 3(b) and 4(b), due to the potential barrier, the carrier density is low near the grain boundary. Figure 5 shows the dependence of the carrier density and potential barrier on the defect density with variations in the grain size. Here, the carrier density in the middle of the grain is plotted. The carrier density and potential barrier are determined from Figs. 2, 3 and 4.

First, the case of a small grain size such as 10 nm is considered using Figs. 2 and 5. For a low defect density such as 1×10^{11}–1×10^{12} cm^{-2}, the potential barrier is low. Since the space-charge regions have not yet reached the middle of the grain, the carrier density is high. However, the carrier density is slightly lower than a dopant density of 1×10^{19} cm^{-3} because the ionization rate is lower than one when the dopant energy is similar to the Fermi level. As the defect density in-

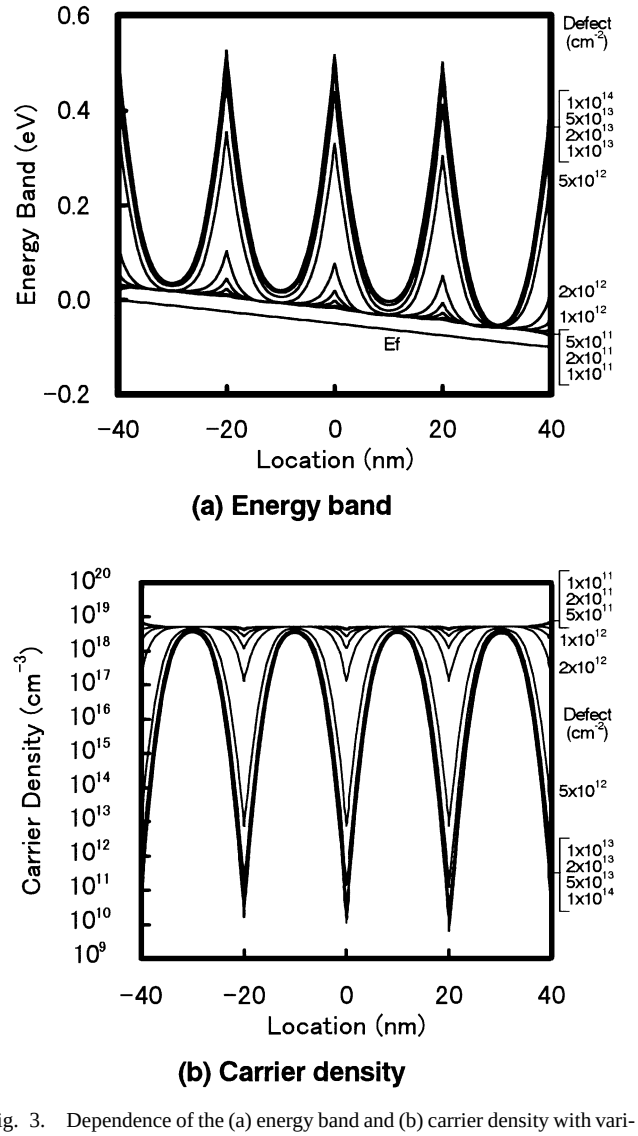

Fig. 3. Dependence of the (a) energy band and (b) carrier density with variations in the defect density for a grain size of 20 nm.

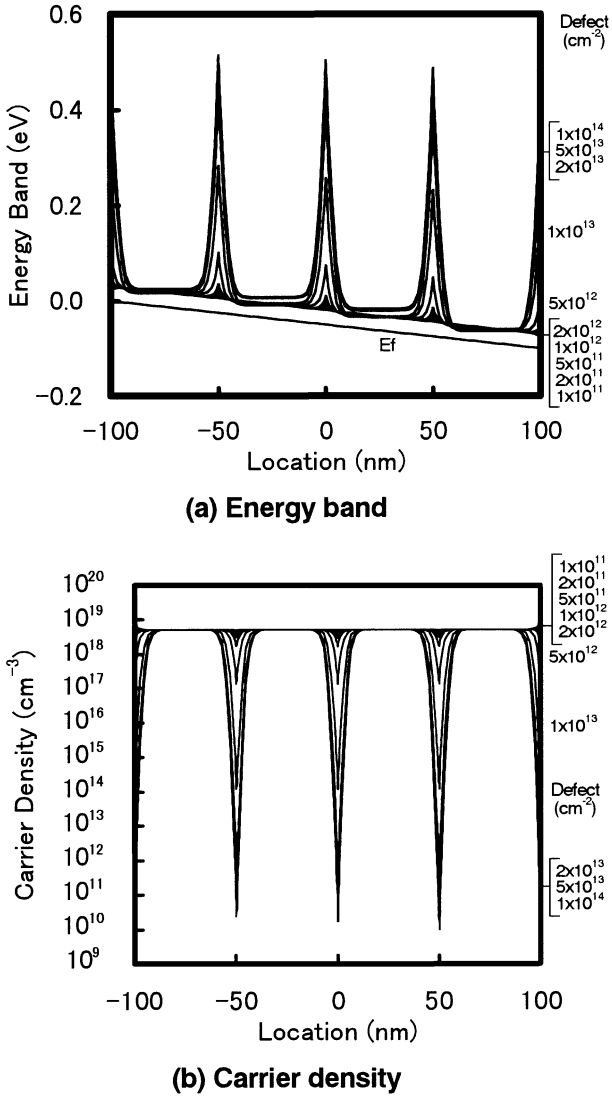

Fig. 4. Dependence of the (a) energy band and (b) carrier density with variations in the defect density for a grain size of 50 nm.

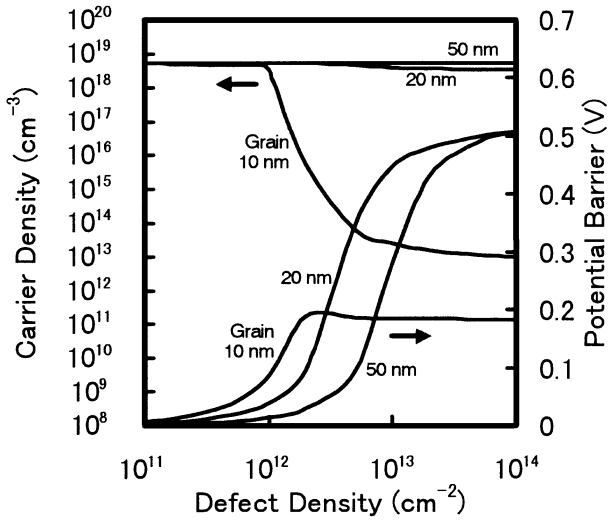

Fig. 5. Dependence of the carrier density and potential barrier on the defect density with variations in the grain size.

creases to 2×10^{12} cm^{-2}, the potential barrier becomes higher. Since the space-charge regions have reached the middle of the grain, the carrier density becomes significantly lower. As the defect density increases to 5×10^{12} cm^{-2}, since the space-charge regions have already spread over the entire grain, neither the charge density nor the width of the space-charge region can change further. Therefore, the potential barrier remains the same. On the other hand, E_c–E_f becomes larger, and the carrier density becomes lower. As the defect density increases to 1×10^{13}–1×10^{14} cm^{-2}, E_c–E_f becomes the highest and remains the same. The reason is as follows. E_c–E_f at the grain boundary becomes so large that the defect energy is similar to the Fermi level. If E_c–E_f at the grain boundary becomes even larger, the defect energy would become higher than the Fermi level, the boundary defects could not trap the free carriers, the potential barrier would become lower, and E_c–E_f at the grain boundary would become lower. Therefore, E_c–E_f at the grain boundary is self-consistently decided to the maximum where the defect energy is similar to the Fermi level. In this case, some of the boundary defects trap the free carriers.

Next, the case of a large grain size such as 50 nm is considered using Figs. 4 and 5. For a low defect density such as 1×10^{11}–2×10^{12} cm^{-2}, the potential barrier is low, and the carrier density is high. As the defect density increases to 5×10^{12}–2×10^{13} cm^{-2}, the potential barriers become higher. However, since the space-charge regions have not yet reached the middle of the grain, the carrier density remains high. As the defect density increases to 5×10^{13}–1×10^{14} cm^{-2}, before the space-charge regions spread over the entire grain, E_c–E_f at the grain boundary reaches its maximum. Therefore, even if the defect density increases further, the potential barrier remains the same, and the carrier density remains high.

Figure 6 shows the dependence of the electric conductivity on the defect density with variations in the grain size. The electric conductivity is determined by the carrier density and potential barrier. The electric conductivity decreases significantly around the specific defect density that depends on the grain size. Roughly speaking, using the analytical method,[6–9] the electric conductivity decreases at the specific defect density that is equal to the dopant density if the boundary defects are assumed to be distributed uniformly throughout the entire poly-Si film. The specific defect densities for the grain size 10 nm, 20 nm and 50 nm are 1×10^{13}, 2×10^{13}, 5×10^{13} cm^{-2}, respectively. Using device simulation, different results have been obtained. This indicates that since the device simulation can handle all the phenomena that are approximated or assumed in analytical methods, more accurate results can be obtained.

4. Extraction of the Defect Density

As seen in Fig. 6, the electric conductivity is sensitive to the defect density. Therefore, it is possible to extract the actual defect density by comparing the simulated electric conductivity to the experimental one. The experiment was performed as follows.[13] First, an amorphous-silicon (a-Si) film 50 nm was formed using low-pressure chemical vapor deposition. Phosphorus atoms 1×10^{19} cm^{-3} were implanted. The a-Si film was crystallized using a XeCl excimer laser with variations in the laser energies of 220 mJ/cm^2, 340 mJ/cm^2 and 460 mJ/cm^2 to fabricate a poly-Si film, and the phosphorus atoms were activated simultaneously. The poly-Si film was patterned and aluminum electrodes were fabricated. The electric conductivity was measured. Next, the grain sizes of the poly-Si films were measured using, for example, tunneling electron microscopy (TEM). The grain sizes for the laser energies of 220 mJ/cm^2, 340 mJ/cm^2 and 460 mJ/cm^2 were 10 nm, 20 nm and 50 nm, respectively. Next, using these grain sizes, the dependence of the electric conductivity on the defect density is simulated using the device simulation shown in Fig. 6. Finally, by comparing the experimental and simulated electric conductivity, the actual defect density can be extracted.

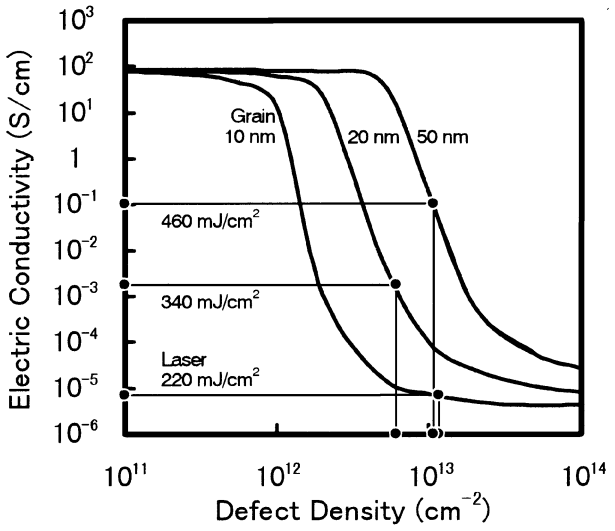

Fig. 6. Dependence of the electric conductivity on the defect density with variations in the grain size, and experimental electric conductivity with variations in the laser energy for crystallization, whose defect density is extracted.

Table I. Laser energy density, grain size, electric conductivity and extracted defect density.

Laser energy (mJ/cm^2)	220	340	460
Grain size (nm)	10	20	50
Electric conductivity (S/cm)	7.0×10^{-6}	1.9×10^{-3}	1.1×10^{-1}
Defect density (cm^{-2})	1.2×10^{13}	0.6×10^{13}	1.1×10^{13}

Figure 6 also shows the experimental electric conductivity with variations in the laser energy for crystallization. From the intersection of the simulated curve and the experimental value, the defect density can be extracted. Table I shows the laser energy density, grain size, electric conductivity and extracted defect density. The extracted defect densities for the laser energies of 220 mJ/cm^2, 340 mJ/cm^2 and 460 mJ/cm^2 are on the order of 10^{13} cm^{-2}. It is very interesting that the defect density can be extracted using very simple devices such as lightly doped poly-Si films and very easy measurements such as those of electric conductivity.

5. Conclusions

Device simulations of grain boundaries in lightly doped poly-Si films have been performed. Dependence of the energy band, carrier density, potential barrier and electric conductivity on the defect density and grain size was carefully investigated. As a result, the mechanism of the carrier trans-

portation has been clarified. The boundary defects not only trap and reduce free carriers, but also form the potential barrier and interfere with the carrier movement. As the defect density increases, in the case of the small grain size, first, the space-charge regions spread over the entire grain. Next, while the potential barrier remains the same, E_c–E_f increases, and the carrier density decreases. Finally, E_c–E_f becomes the highest and remains the same. On the other hand, in the case of the large grain size, before the space-charge regions spread over the entire grain, E_c–E_f at the grain boundary reaches its maximum. Therefore, even if the defect density increases further, the potential barrier remains the same, and the carrier density remains high. By comparing the experimental and simulated electric conductivity, the defect density can be extracted.

Acknowledgements

The authors wish to thank Seiichiro Higashi of the Seiko Epson Corporation and Professor Piero Migliorato of the University of Cambridge. The authors also wish to thank the members of the Base Technology Research Center of the Seiko Epson Corporation, the Epson Cambridge Laboratory, Professor Migliorato's group at the University of Cambridge and the LT Business Development Center of the Seiko Epson Corporation.

1) T. Sameshima, K. Saito, M. Sato, A. Tajima and N. Takashima: Jpn. J. Appl. Phys. **36** (1997) L1360.
2) S. Higashi, K. Ozaki, K. Sakamoto, Y. Kano and T. Sameshima: Jpn. J. Appl. Phys. **38** (1999) L857.
3) T. Sameshima, K. Saitoh, N. Aoyama, S. Higashi, M. Kondo and A. Matsuda: Jpn. J. Appl. Phys. **38** (1999) 1892.
4) S. Higashi: Dig. AM-LCD '99, Tokyo, 1999, p. 225.
5) K. Sakamoto, Y. Tsunoda, T. Watanabe, K. Asada, T. Mohri, T. Sameshima and S. Higashi: Ext. Abstr. (60th Autumn Meet. 1999); The Japan Society of Applied Physics, Tokyo, p. 804 [in Japanese].
6) J. Y. W. Seto: J. Appl. Phys. **46** (1975) 5247.
7) G. Baccarani, B. Ricco and G. Spadini: J. Appl. Phys. **49** (1978) 5565.
8) P. V. Evans and S. F. Nelson: J. Appl. Phys. **69** (1991) 3605.
9) T. Kamins: *Polycrystalline Silicon for Integrated Circuits and Displays* (Kluwer Academic Publishers, Boston, 1998) 2nd ed., Chap. 5, p. 199.
10) S. Selberherr: *Analysis and Simulation of Semiconductor Devices* (Springer-Verlag, Heidelberg, 1984).
11) K. Taniguchi: *Latest Semiconductor Process and Device Simulation Technology* (Realize Inc., Tokyo, 1990).
12) Silvaco International: Device Simulator Atlas.
13) S. Higashi: private communication (2000).